# One-dimensionality in atomic nuclei: A candidate for linear-chain $\alpha$ clustering in $^{14}$C

A. Fritsch,[1,2,3,*] S. Beceiro-Novo,[1,2] D. Suzuki,[1,4] W. Mittig,[1,2] J. J. Kolata,[5] T. Ahn,[1,5] D. Bazin,[1] F. D. Becchetti,[6] B. Bucher,[5,†] Z. Chajecki,[1,‡] X. Fang,[5] M. Febbraro,[6,§] A. M. Howard,[5,‖] Y. Kanada-En'yo,[7] W. G. Lynch,[1,2] A. J. Mitchell,[8,¶] M. Ojaruega,[6] A. M. Rogers,[9,#] A. Shore,[1,2] T. Suhara,[10] X. D. Tang,[5,**] R. Torres-Isea,[6] and H. Wang[11]

[1]*National Superconducting Cyclotron Laboratory, Michigan State University, East Lansing, Michigan 48824, USA*

[2]*Department of Physics and Astronomy, Michigan State University, East Lansing, Michigan 48824, USA*

[3]*Department of Physics, Gonzaga University, Spokane, Washington 99258, USA*

[4]*Institut de Physique Nucléaire, CNRS-IN2P3, Univ. Paris-Sud, Université Paris-Saclay, 91406 Orsay Cedex, France*

[5]*Department of Physics, University of Notre Dame, Notre Dame, Indiana 46556, USA*

[6]*Department of Physics, Randall Laboratory, University of Michigan, Ann Arbor, Michigan 48109, USA*

[7]*Department of Physics, Kyoto University, Kyoto 606-8502, Japan*

[8]*School of Physics and Astronomy, University of Manchester, Manchester M13 9PL, United Kingdom*

[9]*Argonne National Laboratory, 9700 S Cass Ave B109, Lemont, Illinois 60439, USA*

[10]*Matsue College of Technology, Matsue 690-8518, Japan*

[11]*Shanghai Institute of Applied Physics, Chinese Academy of Science, China*

(Received 29 May 2015; published 28 January 2016)

The clustering of $\alpha$ particles in atomic nuclei results in the self-organization of various geometrical arrangements at the femtometer scale. The one-dimensional alignment of multiple $\alpha$ particles is known as linear-chain structure, evidence of which has been highly elusive. We show via resonant elastic and inelastic $\alpha$ scattering of a radioactive $^{10}$Be beam that excited states in the neutron-rich nucleus $^{14}$C agree with recent predictions of linear-chain structure based on an antisymmetrized molecular dynamics model.

DOI: 10.1103/PhysRevC.93.014321

## I. INTRODUCTION

Composite objects in nature often self-assemble into ordered structures that are characterized by their geometry and dimensionality as a reflection of underlying laws and interactions. One such example in atomic nuclei is the formation of $\alpha$-particle clusters, usually near the $\alpha$-decay threshold [1–5]. As early as the 1950s, Morinaga [6,7] conjectured an exotic arrangement of $\alpha$ clusters, today referred to as a "linear-chain structure," in which clusters are one-dimensionally aligned. Modern theories based on realistic interactions including antisymmetrized molecular dynamics (AMD) and fermionic molecular dynamics (FMD) [8–14] have predicted linear-chain states that are stable against bending.

The experimental search for linear-chain structures constitutes a longstanding challenge in nuclear physics. Their large moments of inertia, which affect their quantized rotation, and their strong decay branching to known cluster states are essential signatures of their existence. A rotational band proposed for $^{16}$O [15] and a 46.4 MeV resonance in $^{24}$Mg that decays into a pair of $^{12}$C nuclei in the Hoyle state [16] were suggested as possible candidates, but these interpretations are not definitive [9,17]. Even the simplest case of a $3\alpha$ chain in $^{12}$C remains elusive; although both FMD [10] and AMD [11,12] calculations predict a linear chain of $\alpha$ clusters for the $0_3^+$ state at 10.3 MeV, there has been no experimental confirmation nearly seven decades after Morinaga's conjecture.

From previous studies of $^{10}$Be, where two valence neutrons preserve the $2\alpha$-cluster nature of $^{8}$Be [18,19], we conjectured a linear-chain structure in $^{14}$C, consisting of $^{12}$C and two neutrons. However, models do not agree on the existence of linear-chain states in $^{14}$C [8,20]. Several previous experiments searched for excited states in $^{14}$C [21–24] above the $\alpha$-decay threshold $S_\alpha = 12.01$ MeV. While many levels were identified, numerous spin-parities $J^\pi$ remain unknown or inconsistent, limiting the identification of rotational bands and insight into their intrinsic structures.

## II. EXPERIMENT

To explore the existence of linear-chain states in neutron-rich $^{14}$C, we performed an experiment at the University of Notre Dame that used resonant $\alpha$ scattering to determine $J^\pi$ and decay properties of levels above $S_\alpha$ in $^{14}$C. The experiment was performed by using the prototype active target-time projection chamber (PAT-TPC) [25]. A 46 MeV $^{11}$B($5^+$) primary beam of 1–1.5 $\mu$A bombarded a stack of four 0.1-mg/cm$^2$-thick $^{13}$C targets to produce $^{10}$Be ions that were collected and purified in flight by the *TwinSol* device [26].

*fritscha@gonzaga.edu

†Present address: Lawrence Livermore National Laboratory, Livermore, California 94550, USA.

‡Present address: Department of Physics, Western Michigan University, Kalamazoo, Michigan 49008, USA.

§Present address: Physics Division, Oak Ridge National Laboratory, Oak Ridge, Tennessee 37831, USA.

‖Present address: Department of Physics and Astronomy, Aarhus University, 8000 Aarhus C, Denmark.

¶Present address: Department of Nuclear Physics, Australian National University, Canberra, ACT 2601, Australia.

#Present address: Department of Physics, University of Massachusetts Lowell, Lowell, Massachusetts 01854, USA.

**Present address: Institute of Modern Physics, Lanzhou, China.

 

This secondary beam was delivered to the cylindrical target volume of He : $CO_2$ 90 : 10 gas at 1 atm of the PAT-TPC, measuring 50 cm along the beam axis and 27 cm in diameter. The $^{10}$Be energy was measured to be 39.7 (5) MeV by using silicon detectors. The center-of-mass energy $E_{\mathrm{c.m.}}$ decreased from 11.3 MeV to zero while traveling the length of the gas volume. The average rate of $^{10}$Be that entered the volume was $10^3$ ions per second with a total of $3.2 \times 10^8$. The beam purity was about 35% with main contaminants of $^4$He($2^+$) (50%), $^9$Be($4^+$) (5%), and $^{10}$B($4^+$) (3%).

Electrons from reaction trajectories are guided toward the Micromegas [27] amplifier by an electric field of 0.8 kV/cm parallel to the beam axis. The Micromegas consists of 2-mm-wide radial strips separated into quadrants. A waveform digitizer [28] records the charge as a function of drift time $t_{\mathrm{drift}}$ over 40 $\mu$s by using an array of 511 switching capacitors. We increased the amplification gain of every fifth radial strip to measure the $\alpha$-particle trajectories with lower-energy deposits. The trigger generation required a pair of high-gain strips at radius $r = 12$ mm to receive signals from radially opposed quadrants.

Figure 1(a) shows the recorded charge against $t_{\mathrm{drift}}$ and $r$ for a scattering event of $^{10}$Be from an $\alpha$ particle in the gas, where negative and positive radii represent radially opposed quadrants. The discrete $\alpha$ trajectory is due to the increased sensitivity of the high-gain strips. The laboratory angles $\theta_{\mathrm{lab}}$ and $E_{\mathrm{c.m.}}$ at the reaction vertex were deduced by accounting for energy deposition and the 2.4 cm/$\mu$s electron-drift velocity [25]. Beam particles were differentiated by using the energy loss per unit length obtained from the beam track. Both elastic scattering and inelastic scattering to the $2_1^+$ state of $^{10}$Be at 3.37 MeV were selected by gating on the kinematical correlation of $\theta_{\mathrm{lab}}^{^{10}\mathrm{Be}}$ and $\theta_{\mathrm{lab}}^{\alpha}$ in Fig. 1(b). The events along the $\theta_{\mathrm{lab}}^{^{10}\mathrm{Be}} + \theta_{\mathrm{lab}}^{\alpha} = 90^\circ$ line originate from scattering of $\alpha$-particle contaminants in the beam and in the gas.

## III. RESULTS

States of $^{14}$C were resonantly populated via scattering of a $^{10}$Be beam off $^4$He gas particles. While resonant $\alpha$ scattering is advantageous for its sensitivity to $\alpha$-cluster states that favor decay via $\alpha$ emission [18,19], measurements with a radioactive beam are challenging. A previous study [23,24] suffered

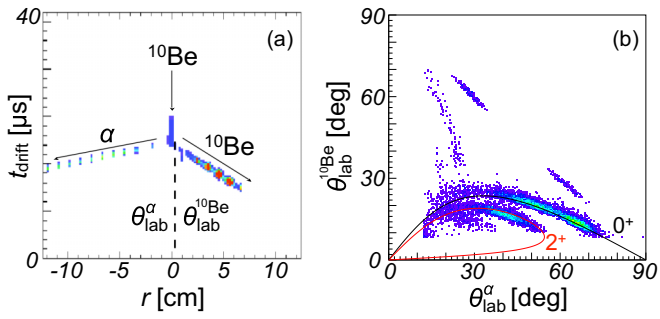


FIG. 1. (a) Trajectories of a $^{10}$Be + $\alpha$ scattering event. (b) $\theta_{\mathrm{lab}}^{^{10}\mathrm{Be}}$ vs $\theta_{\mathrm{lab}}^{\alpha}$ plot with the kinematical curves for elastic and inelastic scattering to the $^{10}$Be $2_1^+$ state. Data shown have been selected via energy-loss gating for $^{10}$Be beam particles.

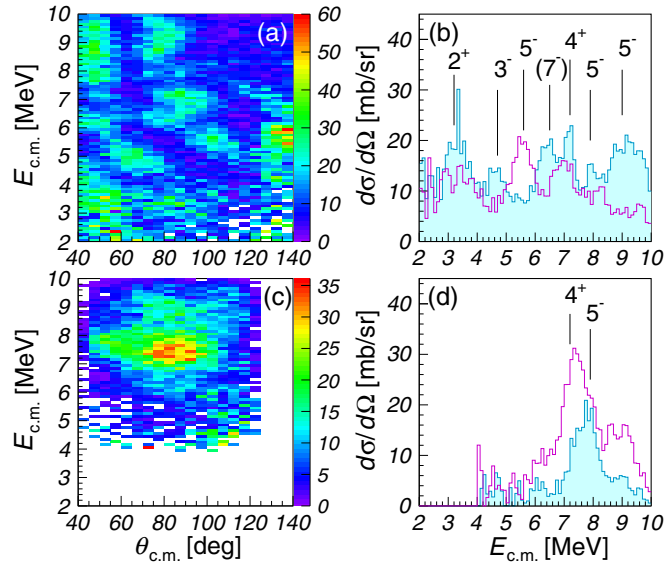


FIG. 2. Differential cross sections of $^{10}$Be scattering off $\alpha$ particles: (a) elastic scattering and (c) inelastic scattering to the $2_1^+$ state of $^{10}$Be. The color scale is given in mb/sr. Excitation functions for (b) elastic and (d) inelastic scattering also are shown. The shaded spectrum is gated by $\theta_{\mathrm{c.m.}} = 70^\circ$–$90^\circ$($45^\circ$–$55^\circ$), and the blank spectrum by $90^\circ$–$110^\circ$ ($70^\circ$–$80^\circ$) for elastic (inelastic) scattering. The lines indicate identified resonances.

limited angular acceptance, uncertainties in reaction-channel selection, and inaccurate energy calibration. By using the newly developed thick target method [19] for the PAT-TPC [25], we measured cross sections for both elastic and inelastic scattering to the $2_1^+$ 3.37 MeV state of $^{10}$Be over a wide range of $\theta_{\mathrm{c.m.}}$ as a continuous function of $E_{\mathrm{c.m.}}$ as shown in Fig. 2. Characteristic diffractive patterns at several energies can be seen in the spectrum for the elastic channel in Fig. 2(a). A total of seven resonances were identified, as indicated in the excitation function of Fig. 2(b).

Each diffractive resonance pattern follows the square of the Legendre polynomial $P_L^2(\theta_{\mathrm{c.m.}})$ for the angular momentum $L$. States with $J^\pi = L^{(-)^L}$ are selectively populated by the $L$ wave because both $\alpha$ and $^{10}$Be are spin-zero. Following previous analyses [18,24], optimal $L$ values were chosen by comparing the angular distributions to $P_L^2$ (Fig. 3). The measured angular domain of $\theta_{\mathrm{c.m.}} = 35^\circ$ to $145^\circ$ is well suited to extract resonance parameters: potential scattering dominates at forward angles, at backward angles $^6$He cluster exchange may be dominant, and there is less selectivity for $L$ values. There is very good agreement in the oscillatory pattern of the data with the proposed polynomials, giving clear $J^\pi$ assignments to the dominant partial-wave contributions of the resonances. We tentatively attribute a ($7^-$) state at 6.5 MeV with a lower-quality fit. More realistic angular distributions were calculated with the $R$-matrix formalism [29] by using optical-model potential parameters based on 48 MeV $\alpha + {}^9$Be elastic-scattering data [30] for a channel radius of 4.7 fm. As one would expect, the experimental distributions are not exactly reproduced due to uncertainties in the optical-model parametrization and the lack of a possible $^6$He transfer

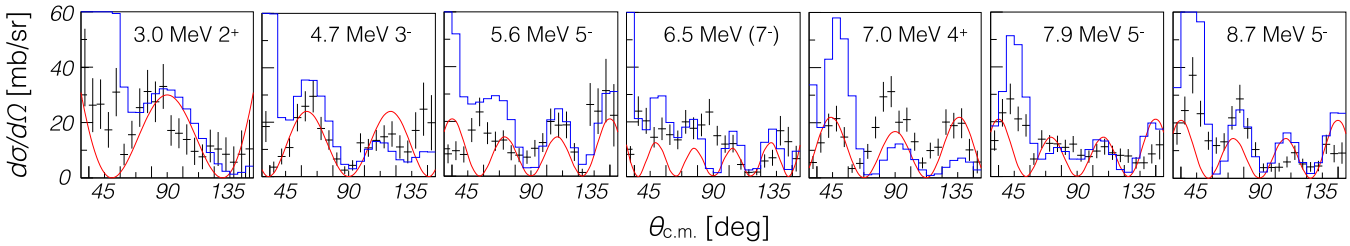


FIG. 3. Differential elastic cross sections for resonances identified in $\alpha + {}^{10}$Be scattering (Fig. 2). The data (crosses) are compared to $P_L^2(\theta_{\text{c.m.}})$ functions (curves) and $R$-matrix calculations (histograms).

component in the calculation, as well as limitations in Monte Carlo simulations for detector efficiency at the limit of angular acceptance. Nonetheless, the diffraction maxima and minima agree closely with the data and the $P_L^2$ curves. The $J^\pi$ assignments thus are reliable and independent of the detailed effects of potential scattering and interference among resonances. Optimized resonance parameters from our analysis are summarized in Table I, where the $^{14}$C excitation energy is given by $E_x = E_{\text{c.m.}} + S_\alpha$. The systematic error of $\pm 0.2$ MeV in $E_{\text{c.m.}}$ arises from uncertainties in beam energy and reaction vertex. The spectroscopic factors $SF$, defined as the ratio of the experimental width and the single-particle width [29], are assigned a conservative $\pm 50\%$ uncertainty because they depend on the transmission factors $|U_{cc}^0|$ that represent the absorption due to the optical potential and are governed by the chosen parametrization. Shown in the last two columns are known $\alpha$-emission levels [22] and $\alpha + {}^{10}$Be elastic resonances [24] that may correspond to the observed states.

The inelastic data in Fig. 2(c) show a strong resonance at $E_{\text{c.m.}} = 7$ to 8 MeV. This resonance consists of branching from the 7.0 MeV $4^+$ and 7.9 MeV $5^-$ resonances, which lack clear separation due to the lower energy resolution for inelastic scattering. This interpretation of the branching is supported by the peak centroid that clearly shifts from the $4^+$ to $5^-$ excitation energies as $\theta_{\text{c.m.}}$ changes from 70°–80° to 45°–55°, as shown in Fig. 2(d). This is consistent with previous studies where proposed (19.07) MeV and 19.83 MeV states were identified in decay spectra to the $^{10}$Be $2_1^+$ state [22].

In Table I, we also compare our data to the previous result of resonant $\alpha$ scattering in Ref. [24]. Accounting for the statistical uncertainty of $\pm 0.02$ MeV and the systematic uncertainty of $\pm 0.175$ MeV for resonances identified in Ref. [24], our resonance energies are consistent with those in Ref. [24] aside from a small $2^+$ resonance at 17.97 MeV and the possible mixing of $7^-$ and $4^+$ states in their resonance at 18.82 MeV. While spin and parity assignments disagree for some states, the results differ only by $\Delta L = 1$. Since our assignments are based on diffractive patterns over wide angular ranges, they should be reliable, whereas the assignments in Ref. [24] were made over a very limited angular range from 5° to 13.5° in the laboratory frame, or 153° to 170° in the center-of-mass frame. In Ref. [24], while the $R$-matrix fit to the excitation function measured at $\theta_{\text{c.m.}} = 180°$ is reasonable, the absolute cross sections of the experimental data were normalized to the Rutherford scattering cross section at the lowest yield, making the results from the $R$-matrix analysis highly dependent on the nuclear potential scattering component and the transfer component of the reaction.

TABLE I. Summary of resonances and their properties deduced via $\alpha + {}^{10}$Be elastic scattering. Known $\alpha$-emission levels [22] and $\alpha + {}^{10}$Be elastic scattering resonances [24] at nearby energies are listed in the last two columns.

| $E_{\text{c.m.}}$ [MeV] | $E_x$ [MeV] | $J^\pi$ | $\lvert U_{cc}^0\rvert$ | $\Gamma_\alpha$ [MeV] | $SF$ | $E_x$ [22] [MeV] | $E_x$, $J^\pi$ [24] [MeV] |
|---|---|---|---|---|---|---|---|
| 3.0 | 15.0 | $2^+$ | 0.50 | 0.29 | 0.3 | 14.8(1) | |
| 4.7 | 16.7 | $3^-$ | 0.40 | 0.27 | 0.2 | 16.43(10) | |
| 5.6 | 17.6 | $5^-$ | 0.85 | 0.10 | 0.4 | 17.3(1) | 17.32, $3^-$ |
| 6.5 | 18.5 | $(7^-)$ | 0.95 | 0.02 | 1.6 | 18.5(1) | |
| 7.0 | 19.0 | $4^+$ | 0.35 | 0.34 | 0.2 | (19.07(1)) | 18.82, $5^-$ |
| 7.9 | 19.9 | $5^-$ | 0.50 | 0.10 | 0.1 | 19.83(1) | 19.67, $5^-$ |
| 8.7 | 20.7 | $5^-$ | 0.40 | 0.57 | 0.4 | 20.6(1) | 20.80, $6^+$ |

## IV. DISCUSSION

Currently, the only theoretical model that provides quantitative predictions that can be compared to our data is the $\beta$-$\gamma$ constraint AMD model [8]. We compare the model predictions to our data for positive-parity states in Fig. 4(a); a similar comparison to negative-parity states is not made since neither our data nor the AMD model show rotational bands for such states [8]. A series of AMD states starting near 3 MeV above $S_\alpha$ are attributed to rotation of a $3\alpha$ linear chain. The linear alignment of $3\alpha$ clusters and the localization of $2n$ are clearly seen in the density distributions. A positive-parity rotational band (II) was previously associated with a linear structure due to its narrow level spacing [21]. It is, however, about 5 MeV lower than the predicted energy, and its level spacing is much narrower than the prediction. Conversely, the level energies of the $2^+$ and $4^+$ states of this work (I) agree with the corresponding rotational members of the predicted band (IV). Furthermore, the $2^+$ and $4^+$ $SF$ values are consistent with the sizable overlaps of the AMD states with a $^{10}$Be$(0_1^+) + \alpha$ cluster wave function (28% for $2^+$ and 16% for $4^+$) [31]. This supports the assignment of the observed positive-parity states as a $3\alpha$ linear-chain rotational band in $^{14}$C. While there is a previous suggestion of doublet partnering of positive- and negative-parity bands [21], only a positive-parity band structure is identified in our study, in line with AMD predictions for linear-chain structure [8].

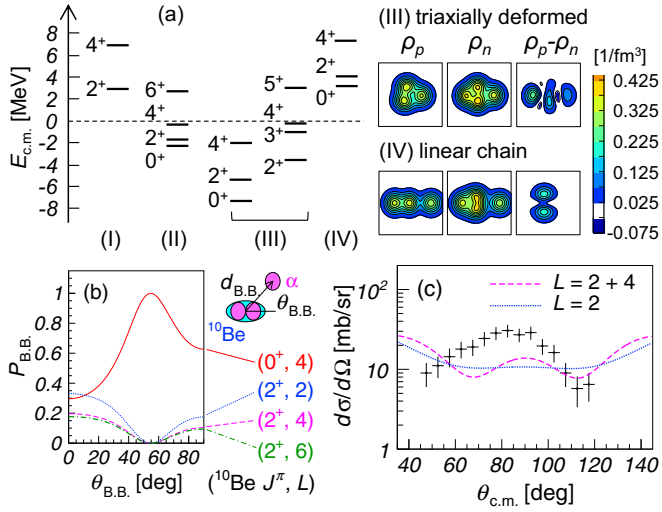


FIG. 4. Comparison with theoretical predictions: (a) Energy levels of positive-parity states in $^{14}$C relative to $S_\alpha$; shown are (I) present results, (II) a previously suggested positive-parity band [21], and (III) triaxially deformed and (IV) linear-chain levels predicted by the $\beta$-$\gamma$ constraint AMD method [8]. Predicted distributions of proton density $\rho_p$, neutron density $\rho_n$, and their differential $\rho_p - \rho_n$ in $10 \times 10$ fm$^2$ boxes also are shown. (b) $P_{B.B.}$ vs $\theta_{B.B.}$ plot of the Brink–Bloch wave function for the $^{14}$C $4^+$ state. The results for $^{10}$Be($0^+$) with $L = 4$ (solid line), $^{10}$Be($2^+$) with $L = 2$ (dotted line), $^{10}$Be($2^+$) with $L = 4$ (dashed line), and $^{10}$Be($2^+$) with $L = 6$ (dash-dotted line) are displayed. The geometrical arrangements of $^{10}$Be + $\alpha$ clusters for an arbitrary $\theta_{B.B.}$ are schematically shown above the $L$ labels. (c) Inelastic cross section gated by $E_{c.m.} = 7.0$–$7.5$ MeV. The data are compared to $R$-matrix calculations assuming only $L = 2$ (dotted line) and mixing $L = 2,4$ (dashed line).

Another indicator of the linear-chain structure is the large cross section in the inelastic channel of the $2_1^+$ state of $^{10}$Be. The overlap of the linear-chain $4^+$ state with the $^{10}$Be $2_1^+$ state (28%) is predicted to be comparable to that of the $0_1^+$ state (16%) [31]. This agrees with the inelastic excitation function in Fig. 2(d), where the $4^+$ state's resonance strength is comparable to the elastic. To examine the sensitivity of the inelastic component to the $3\alpha$ configuration geometry, we studied a Brink–Bloch wave function [32] consisting of an axially deformed $^{10}$Be cluster and an $\alpha$ particle separated by a distance $d_{B.B.}$ with an angle $\theta_{B.B.}$ to the symmetry axis of $^{10}$Be, illustrated in Fig. 4(b). The linear-chain state can be roughly approximated by $d_{B.B.} = 5$ fm and $\theta_{B.B.} = 0$. The probabilities $P_{B.B.}$ of the $^{10}$Be($0^+$) and $^{10}$Be($2^+$) states with different partial waves of the intercluster motion were estimated for $4^+$ states projected from the Brink–Bloch wave function. The calculated $P_{B.B.}$ in Fig. 4(b) reveal strong $\theta_{B.B.}$ dependence. Since the ratio of inelastic components to the elastic component increases as $\theta_{B.B.}$ diminishes and is maximal at $\theta_{B.B.} = 0$ where $3\alpha$ clusters are fully aligned, the measured strong branching to the $^{10}$Be($2^+$) state favors a linear-chain assignment for the observed rotational band.

Figure 4(c) compares the inelastic angular distribution at $E_{c.m.} = 7.0$–$7.5$ MeV to $R$-matrix calculations, one assuming only $L = 2$ and the other mixing $L = 2$ and 4 with $SF$ values proportional to $P_{B.B.}$. A description without nonresonant components and absorption was adopted. The $L = 6$ component was not taken into account due to its much lower penetrability. The data have a broad maximum centered at 90° that is not reproduced by $L = 2$. The predicted mixture with $L = 4$ increases the cross section at 90° and qualitatively describes the features seen in the data.

A different prediction made with the molecular orbital model expects the $^{14}$C linear-chain structure to be energetically unstable [20]. In this picture, while the presence of the two valence neutrons keeps the $3\alpha$ cluster from breaking up, the calculated energy surface is nearly constant with respect to bending angles. The AMD model predicts similar characteristics for the energy surface, but it further incorporates configuration mixing [8]. The inclusion of configuration mixing is central to the stabilization of the linear-chain structure in the AMD model because it results in the appearance of states with triaxial configurations at lower energies, as shown in Fig. 4(a). It is in these triaxially deformed states that the bending $3\alpha$ configurations exist, allowing the linear-chain states to form stable and pure geometrical linear configurations at higher energies since the triaxial and linear-chain states are orthogonal. Without the triaxially deformed states, the bending $3\alpha$ configurations would mix with the linear-chain configuration, rendering it unstable. Thus, the orthogonality between the different geometrical states makes the linear chain in $^{14}$C robust and allows high-spin states via rotation. In contrast, $^{12}$C has neither the valence neutrons needed for stronger bonding nor triaxial bands [11]. While its low-lying $0^+$ state may form a linear-chain configuration, the chain is fragile and readily bends and collapses in $2^+$, $4^+$, and higher spin states, perhaps explaining why linear-chain states in $^{12}$C have yet to be found. The present result thus corroborates the picture that the orthogonality between quantum states is crucial for the one-dimensional self-organization of atomic nuclei and also reveals that the stabilization mechanism of the exotic cluster structures is likely due to excess neutrons.

## V. SUMMARY

We unambiguously identified $2^+$ and $4^+$ resonances in $^{14}$C above the $^{10}$Be + $\alpha$ threshold. We observed a strong decay branch of the $4^+$ resonance to the inelastic channel. Although not expected from simple penetrability arguments, a strong $L = 4$ component of the inelastic branching was necessary to describe the angular distribution. All these independent observables semiquantitatively agree with $\beta$-$\gamma$ constraint AMD predictions [8], supporting the existence of linear-chain structure in $^{14}$C. Although the uniqueness of this interpretation is difficult to ascertain given the comparison to only one model, predictions on level energies and decay properties from other theoretical frameworks are desirable but currently lacking. In particular, predictions from the weakly coupled $\alpha + ^{10}$Be rotating dinuclear model will be important. The argument for linear-chain structure will not be complete until this dinuclear picture that has long been debated in linear-chain states such as $^{24}$Mg [16,17] is ruled out. Furthermore, while experimentally challenging, measurement of the band head $0^+$ state would

greatly inform our linear-chain interpretation. The $0^+$ state is expected to lie 1 MeV below the $2^+$ state, which would be near $E_{\text{c.m.}} = 2$ MeV. However, this energy was at the limit of our trigger cutoff. Future measurements providing additional information on other band states, particularly the band head, are desired.


## ACKNOWLEDGMENTS

We thank F. Abu–Nimeh, N. Usher, and J. Yurkon of the NSCL for their technical support, V. Zelevinsky for helpful discussions, and A.L. Roberts for experimental contributions. The work was partly supported by the US National Science Foundation under Grants No. MRI09-23087 and No. PHY09-69456.



[1] D. Dennison, Energy levels of the $O^{16}$ nucleus, Phys. Rev. **96**, 378 (1954).

[2] K. Ikeda, N. Takigawa, and H. Horiuchi, The systematic structure-change into the molecule-like structures in the self-conjugate $4n$ nuclei, Prog. Theor. Phys. Suppl. **68**, 464 (1968).

[3] Y. Kanada-En'yo and H. Horiuchi, Structure of light unstable nuclei studied with antisymmetrized molecular dynamics, Prog. Theor. Phys. Suppl. **142**, 205 (2001).

[4] A. Tohsaki, H. Horiuchi, P. Schuck, and G. Röpke, Alpha Cluster Condensation in $^{12}$C and $^{16}$O, Phys. Rev. Lett. **87**, 192501 (2001).

[5] J-P. Ebran, E. Khan, T. Nikšić, and D. Vretenar, How atomic nuclei cluster, Nature (London) **487**, 341 (2012).

[6] H. Morinaga, Interpretation of some of the excited states of $4n$ self-conjugate nuclei, Phys. Rev. **101**, 254 (1956).

[7] H. Morinaga, On the spin of a broad state around 10 MeV in $^{12}$C, Phys. Lett. **21**, 78 (1966).

[8] T. Suhara and Y. Kanada-En'yo, Cluster structures of excited states in $^{14}$C, Phys. Rev. C **82**, 044301 (2010).

[9] Y. Suzuki, H. Horiuchi, and K. Ikeda, Study of $\alpha$ chain states through their decay widths, Prog. Theor. Phys. **47**, 1517 (1972).

[10] T. Neff and H. Feldmeier, Cluster structures within fermionic molecular dynamics, Nucl. Phys. A **738**, 357 (2004).

[11] Y. Kanada-En'yo, The structure of ground and excited states of $^{12}$C, Prog. Theor. Phys. **117**, 655 (2007).

[12] T. Suhara, and Y. Kanaka-En'yo, Quadrupole deformation $\beta$ and $\gamma$ constraint in a framework of antisymmetrized molecular dynamics, Prog. Theor. Phys. **123**, 303 (2010).

[13] J. A. Maruhn, N. Loebl, N. Itagaki, and M. Kimura, Linear-chain structure of three $\alpha$ clusters in $^{16}$C and $^{20}$C, Nucl. Phys. A **833**, 1 (2010).

[14] T. Ichikawa, J. A. Maruhn, N. Itagaki, and S. Ohkubo, Linear Chain Structure of Four-$\alpha$ Clusters in $^{16}$O, Phys. Rev. Lett. **107**, 112501 (2011).

[15] P. Chevallier, F. Scheibling, G. Goldring, I. Plesser, and M. W. Sachs, Breakup of $^{16}$O into $^{8}$Be and $^{8}$Be, Phys. Rev. **160**, 827 (1967).

[16] A. H. Wuosmaa, R. R. Betts, B. B. Back, M. Freer, B. G. Glagola, T. Happ, D. J. Henderson, P. Wilt, and I. G. Bearden, Evidence for Alpha-Particle Chain Configurations in $^{24}$Mg, Phys. Rev. Lett. **68**, 1295 (1992).

[17] Y. Hirabayashi, Y. Sakuragi, and Y. Abe, $3\alpha + 3\alpha$ and $3\alpha + {}^{12}$C Configurations in $^{24}$Mg, Phys. Rev. Lett. **74**, 4141 (1995).

[18] M. Freer, E. Casarejos, L. Achouri, C. Angulo, N. I. Ashwood, N. Curtis, P. Demaret, C. Harlin, B. Laurent, M. Milin, N. A. Orr, D. Price, R. Raabe, N. Soić, and V. A. Ziman, $\alpha : 2n : \alpha$ Molecular Band in $^{10}$Be, Phys. Rev. Lett. **96**, 042501 (2006).

[19] D. Suzuki *et al.*, Resonant $\alpha$ scattering of $^{6}$He: Limits of clustering in $^{10}$Be, Phys. Rev. C **87**, 054301 (2013).

[20] N. Itagaki, S. Okabe, K. Ikeda, and I. Tanihata, Molecular-orbital structure in neutron-rich C isotopes, Phys. Rev. C **64**, 014301 (2001).

[21] W. von Oertzen *et al.*, Search for cluster structure of excited states in $^{14}$C, Eur. Phys. J. A **21**, 193 (2004).

[22] P. J. Haigh *et al.*, Measurement of $\alpha$ and neutron decay widths of excited states of $^{14}$C, Phys. Rev. C **78**, 014319 (2008), and references therein.

[23] J. D. Malcolm *et al.*, Study of states in $^{14}$C via the $^{10}$Be($^{4}$He,$^{4}$He)$^{10}$Be, J. Phys.: Conf. Ser. **381**, 012077 (2012).

[24] M. Freer *et al.*, Resonances in $^{14}$C observed in the $^{4}$He($^{10}$Be ,$\alpha$)$^{10}$Be reaction, Phys. Rev. C **90**, 054324 (2014).

[25] D. Suzuki *et al.*, Prototype AT-TPC: Toward a new generation active target time projection chamber for radioactive beam experiments, Nucl. Instrum. Methods Phys. Res., Sect. A **691**, 39 (2012).

[26] F. Becchetti *et al.*, The *TwinSol* low-energy radioactive nuclear beam apparatus: Status and recent results, Nucl. Instrum. Methods Phys. Res., Sect. A **505**, 377 (2003).

[27] Y. Giomataris, Ph. Rebourgeard, J. P. Robert, and G. Charpak, MICROMEGAS: A high-granularity position-sensitive gaseous detector for high particle-flux environments, Nucl. Instrum. Methods Phys. Res., Sect. A **376**, 29 (1996).

[28] P. Baron, D. Calvet, E. Delagnes, X. de la Broise, A. Delbart, F. Druillole, E. Mazzucato, E. Monmarthe, F. Pierre, and M. Zito, AFTER, an ASIC for the Readout of the large T2K time projection chambers, IEEE Trans. Nucl. Sci. **55**, 1744 (2008).

[29] A. M. Lane and R. G. Thomas, *R*-matrix theory of nuclear reactions, Rev. Mod. Phys. **30**, 257 (1958).

[30] T. Y. Li and B. Hird, Analysis of the $C^{12}(p,\alpha)B^{9}$ reaction at 44.5 MeV, Phys. Rev. **174**, 1130 (1968).

[31] T. Suhara and Y. Kanada-En'yo, in *Hadron and Nuclear Physics 09*, edited by A. Hosaka, T. Myo, H. Nagahiro, and K. Nawa (World Scientific, Singapore, 2010), pp. 366–369.

[32] D. M. Brink, in *Proceedings of the International School of Physics "Enrico Fermi," Course XXXVI*, edited by C. L. Bloch (Academic Press, New York, 1966), p. 247.